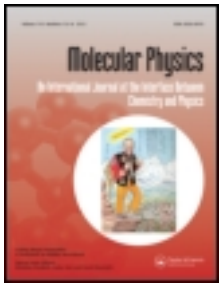

Molecular Physics: An International Journal at the Interface Between Chemistry and Physics
Publication details, including instructions for authors and subscription information:
http://www.tandfonline.com/loi/tmph20

Multicolor stimulated Raman scattering microscopy

Fa-Ke Lu [a], Minbiao Ji [a], Dan Fu [a], Xiaohui Ni [a], Christian W. Freudiger [a], Gary Holtom [a] & X. Sunney Xie [a]

[a] Department of Chemistry and Chemical Biology, Harvard University, Cambridge, MA 02138, USA

Accepted author version posted online: 17 May 2012. Version of record first published: 14 Jun 2012

To cite this article: Fa-Ke Lu, Minbiao Ji, Dan Fu, Xiaohui Ni, Christian W. Freudiger, Gary Holtom & X. Sunney Xie (2012): Multicolor stimulated Raman scattering microscopy, Molecular Physics: An International Journal at the Interface Between Chemistry and Physics, 110:15-16, 1927-1932

To link to this article: http://dx.doi.org/10.1080/00268976.2012.695028

Molecular Physics
Vol. 110, Nos. 15–16, 10–20 August 2012, 1927–1932

Taylor & Francis
Taylor & Francis Group

INVITED ARTICLE

Multicolor stimulated Raman scattering microscopy

Fa-Ke Lu, Minbiao Ji, Dan Fu, Xiaohui Ni, Christian W. Freudiger, Gary Holtom and X. Sunney Xie*

Department of Chemistry and Chemical Biology, Harvard University, Cambridge, MA 02138, USA

(*Received 31 January 2012; final version received 6 May 2012*)

Stimulated Raman scattering (SRS) microscopy has opened up a wide range of biochemical imaging applications by probing a particular Raman-active molecule vibrational mode in the specimen. However, the original implementation with picosecond pulse excitation can only realize rapid chemical mapping with a single Raman band. Here we present a novel SRS microscopic technique using a grating-based pulse shaper for excitation and a grating-based spectrograph for detection to achieve simultaneous multicolor SRS imaging with high sensitivity and high acquisition speeds. In particular, we use a linear combination of the measured CH_2 and CH_3 stretching signals to map the distributions of protein and lipid contents simultaneously.

Keywords: coherent Raman scattering; stimulated Raman scattering; multicolor; grating; pulse shaper

1. Introduction

Stimulated Raman scattering (SRS) microscopy has been developed as a powerful tool for label-free chemical imaging with high chemical specificity and high acquisition speeds up to video rate [1–10]. In SRS microscopy, the sample is coherently excited by two lasers: one is the pump beam with frequency ω_p and the other is the Stokes beam with frequency ω_S. When the beat frequency $\Delta\omega = \omega_p - \omega_S$ is equal to a particular Raman-active molecular vibration of the sample, SRS signals, including both stimulated Raman loss (SRL) and stimulated Raman gain (SRG), are generated due to the nonlinear interaction between the photons and the molecules [11]. SRS is free from the non-resonant background, exhibits an identical spectrum as the spontaneous Raman, and is linearly proportional to the concentration of the analyte, and therefore allows straightforward quantification with SRS. All of these features make SRS a more desirable analytical tool than CARS [12].

In the original implementation of SRS microscopy, two transform-limited picosecond (ps) lasers with narrow spectral bandwidth were used to excite a single Raman-active vibrational mode for fast imaging with high spectral resolution [5]. However, with this ps–ps excitation scheme, other vibrational modes of the sample are not excited, which fails to utilize the full advantage of the rich Raman spectroscopic information and therefore it is not possible to distinguish mixed chemical species with overlapped Raman bands in the sample. For quantitative analysis, such as the concentration ratios between different chemical compounds, multicolor imaging with multiple chemical contrasts is highly desirable. Furthermore, simultaneous mapping of different chemical species in the same sample is extremely important for the investigation of the co-distribution or dynamic correlation between pairs of biomolecules in many *in vivo* biological and biomedical applications [13]. In addition, since the cross phase modulation signal and two-color two-photon absorption (TPA) from pigments or blood may exist as a global non-Raman background in SRS, additional contrast away from any Raman resonance is mandatory in order to remove the background for acute quantitative investigations [14].

To image different Raman modes of the sample, a simple way is to tune the frequency of the pump beam or the Stokes beam in sequential scans [15]. However, this wavelength-tuning approach may lose the co-localization information of different Raman modes, especially when the sample is in a dynamic environment. Spectrally tailored excitation SRS (STE-SRS) microscopy realizes highly specific imaging of a particular chemical species in the presence of interfering species by spectral modulation of a broadband pump beam at high frequency, allowing detection of the SRS signals of the narrowband Stokes beam with high sensitivity [16]. However, with this method, only one chemical contrast is obtained for each scanning. To image other chemical species, another

*Corresponding author. Email: xie@chemistry.harvard.edu

ISSN 0026–8976 print/ISSN 1362–3028 online

http://dx.doi.org/10.1080/00268976.2012.695028
http://www.tandfonline.com

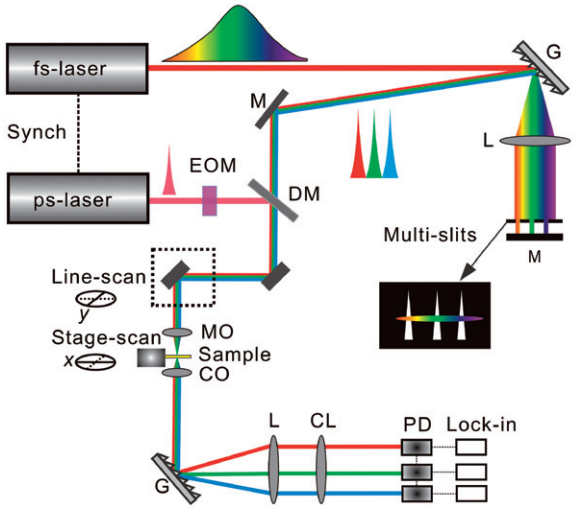

Figure 1. Schematic diagram of the experimental setup for simultaneous multicolor SRS microscopy. A broadband femtosecond (fs) laser source is synchronized to a narrowband picosecond laser. The fs pulse is tailored into a comb-shape spectrum with multi-peaks using a grating-based pulse shaper, each of which corresponds to a particular Raman-active molecular vibrational frequency. A grating-based spectrograph scheme is used to disperse the multi-peaks into different directions and the SRL signals are detected by a home-made photodiode array with parallel lock-in demodulators. G, grating; CL, cylindrical lens; L, lens; M, mirror; DM, dichroic mirror; EOM, electro-optic modulator; MO, microscopic objective; CO, condenser; PD, photodiode.

unique mask has to be designed and used for the spectral manipulation. Multiplex SRS microscopy with the double-modulation and double-demodulation approach based on a multichannel acousto-optical tunable filter (AOTF) device realized multicolor imaging with multiple chemical contrasts for quantitative determination of different chemical species [17]. Unfortunately, the scanning speed is limited by the secondary frequency modulation and demodulation procedure.

In this paper, we present a multicolor SRS microscopic imaging technique with the integration of grating-based spectral manipulation and grating-based spectrographic detection. Using this approach, multicolor images with highly specific multiple chemical contrasts are acquired in parallel with high acquisition speeds (typically ~1.2 s per frame of a 512 × 512 image). A narrowband ps laser (Stokes beam) and a broadband femtosecond (fs) laser (pump beam) are synchronized. The fs beam is spectrally tailored into a comb-shape spectrum with a few narrowband peaks using a grating-based pulse shaper. The Stokes beam is amplitude modulated at a high frequency (~10 MHz). A grating-based spectrograph in the detection path after the condenser is used to disperse the several peaks into different directions. The SRL signal in each spectral peak of the pump beam is measured by an independent photodiode followed by a phase-sensitive lock-in amplifier. We demonstrate the technique by imaging a mixture of polystyrene (PS) and poly(methyl methacrylate) (PMMA) beads. Using a linear combination of the measured CH_2 and CH_3 stretching signals, we were able to map the distributions of the protein and lipid contents simultaneously in mouse ear skin tissue.

2. Experiments

The experimental setup for the multicolor SRS microscopy is shown in Figure 1. A broadband fs Ti:Sapphire laser source (Mira 900D, Coherent Inc.) is synchronized to a narrowband ps Nd:YVO4 laser (High-Q, picoTRAIN) with a Synchrolock system (Coherent Inc.). The broadband fs laser beam (700 mW, FWHM ~18 nm) is delivered into a reflection-configured grating-based pulse shaper [16,18]. An opaque amplitude mask with pre-designed triangular multi-slits is placed on the focal plane of the spectrum dispersed by the grating (inset of Figure 1) to generate a comb-shape spectrum with multi-narrowband peaks. The horizontal position of the slit determines the central wavelength of each peak, while the width of the slit determines the spectral bandwidth and the average optical power of each peak. By adjusting the height of the mask, a balance between the bandwidth and the power of each peak can be achieved. Alternatively, a liquid crystal spatial light modulator (SLM) can be used for convenient adjustment of different spectral patterns [16]. In our experiment, up to three spectral peaks are used. The comb-shape spectrum (pump beam) is collinearly combined with the synchronized ps laser beam (Stokes beam) on a dichroic mirror and delivered into a modified laser scanning microscope (FV300, Olympus). The ps pulses at 1064 nm are amplitude modulated by the electro-optic modulator (EOM) with a polarizer at high frequency (~10 MHz). In the detection part, another grating is used to spatially disperse the three peaks, which are collected by a cylindrical lens and detected by a photodiode array, followed by home-made lock-in amplifiers for multicolor SRL detection [2]. No optical blocking filter is needed because the Stokes beam at 1064 nm is diffracted into a much larger angle compared with the multi-peaks in the pump beam.

In a typical laser-scanning microscope, two-dimensional (2D) imaging is often realized through beam scanning with 2D galvo mirrors. However, in our setup, scanning of the laser beam with large amplitude along the spectral dispersion direction may result in

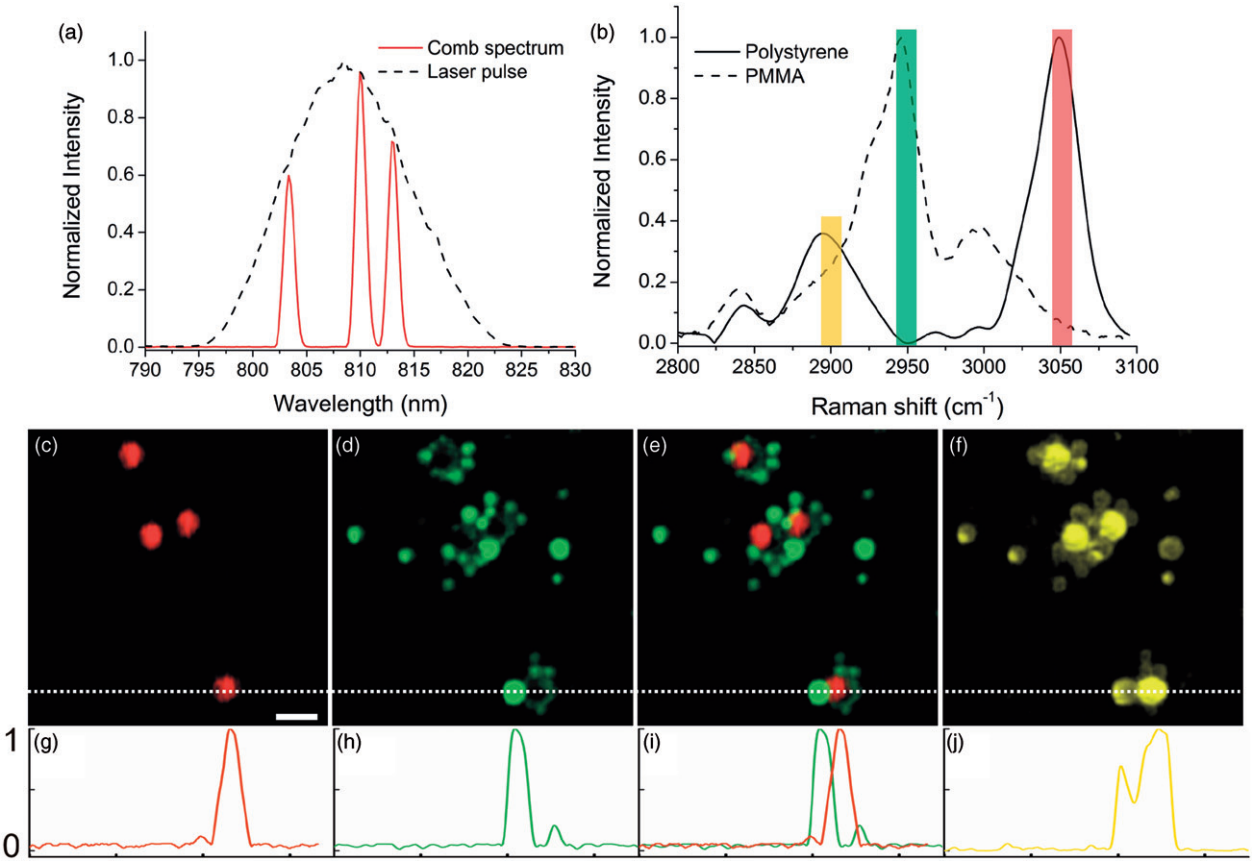

Figure 2. (a) Representative spectra of the femtosecond laser pulse before and after the grating-based pulse shaper. (b) Raman spectra of polystyrene (PS) and poly(methyl methacrylate) (PMMA). The color bars indicate the Raman frequencies selected for the simultaneous three-color imaging of mixed 6 μm PS and 1–5 μm PMMA beads as shown in (c)–(f). (c) At 3054 cm^{-1}, only PS beads produce strong SRS signals (red). (d) At 2950 cm^{-1}, only PMMA beads are visible (green). (e) Overlay of (c) and (d). (g)–(j) Normalized intensity profile across the lines indicated in (c)–(f). (f) At 2900 cm^{-1}, both PS and PMMA beads are visible (yellow), respectively. The average power of each peak in the comb-shape spectrum of the sample is ~8 mW. The scale bar is 10 μm.

spatial crosstalk among adjacent channels, thus limiting the effective imaging field of view. We resolved this problem by replacing 2D beam scanning with a strip scanning method: a motorized sample stage moves along the spectral dispersion direction at a constant speed, while the beam scans along the perpendicular direction in the line-scan mode. The motion of the beam in one direction was minimized by a cylindrical lens and therefore there is no effect on the imaging quality. The whole system is synchronized and operated by Labview programming. For mosaic laser confocal imaging, the strip scanning method is three times as fast as the traditional 2D scanning [19].

3. Results

Figure 2(a) shows spectra of the fs laser pulse before and after passing through the grating-based pulse shaper. Three narrowband peaks are obtained. Note that there are no sidelobe or crosstalk features. The central frequencies of the three peaks are selected to detect the corresponding Raman shift of interest. The bandwidth of the peaks determines the spectral resolution of our system. In principle, the narrower the bandwidth, the higher the spectral resolution of the SRS chemical selective imaging we can achieve. However, narrowing the bandwidth means lowering the optical power. In our experiment, we balance the spectral resolution (~10–20 cm^{-1}) and the average power (~8–15 mW for each peak of the sample). We first characterized our system by imaging a mixture of 6 μm polystyrene (PS) beads and 1–5 μm poly(methyl methacrylate) (PMMA) beads spin-coated on a cover glass. The spontaneous Raman spectra of the two types of beads are shown in Figure 2(b), with the three pre-selected bands indicated by the color bars, and their corresponding SRS images are shown in

Figures 2(c)–(e). In Figure 2(c), at 3054 cm^{-1}, only PS beads produce strong signals, while PMMA beads are almost invisible, as demonstrated by the line intensity profile in Figure 2(g); in Figure 2(d), at 2950 cm^{-1}, only PMMA beads are visible (Figure 2(h)); and in Figure 2(f), at 2900 cm^{-1}, both of the beads are visualized. Figure 2(e) is the overlay of Figures 2(c) and (d), which matches well with Figure 2(f), confirmed by the line profiles as shown in Figures 2(i) and (j). These representations can be explained by the characteristic Raman intensities of PS and PMMA at the three frequencies, as shown in Figure 2(b). Further quantitative analysis is also possible to distinguish pure chemical species from the mixed analyte. These results validate the multi-contrast capability and chemical specificity of our system. In addition, it is worthy of note that since the three-color images are acquired simultaneously, this approach provides perfect co-localized information from the specimen, even though some parts of the sample may move during imaging.

Since SRS exhibits linear concentration dependence, it is possible to quantitatively distinguish different chemical species with overlapped Raman bands, assuming that each chemical species has characteristic Raman features and the calibration data from each pure species are available. In a mixture of m chemical species, the detected multicolor SRS signals from n channels (S_n) can be expressed as

$$S_n = \sum_{m=1}^{M} c_m \cdot k_{m,n},$$
$$k_{m,n} = a \cdot \int \sigma_{m,n}(\omega_{p,n} - \omega_S) \cdot E(\omega_{p,n}) \cdot E(\omega_S)\, d\omega_{p,n}\, d\omega_S, \quad (1)$$

where c_m and $\sigma_{m,n}$ are, respectively, the concentration and the Raman cross section of a particular chemical species within a certain channel for multicolor imaging. m, as an integer from 1 to M, denotes different chemical species, while n, as an integer from 1 to N, denotes different channels. ω_p and ω_S are the pump and Stokes optical fields. α is a constant. The bundled parameter $k_{m,n}$ is equal to the integration of the Raman cross section and the excitation optical fields. For simplicity, we define the matrix associated with $k_{m,n}$ as

$$T = \begin{bmatrix} k_{1,1} & k_{2,1} & \cdots k_{M,1} \\ k_{1,2} & k_{2,2} & \cdots k_{M,2} \\ \vdots & \vdots\cdots & \vdots \\ k_{1,N} & k_{2,N} & \cdots k_{M,N} \end{bmatrix}, \quad (2)$$

and therefore the concentration of m chemical species can be calculated using the equation

$$\begin{bmatrix} c_1 \\ c_2 \\ \vdots \\ c_M \end{bmatrix} = T^{-1} \cdot \begin{bmatrix} S_1 \\ S_2 \\ \vdots \\ S_N \end{bmatrix}, \quad (3)$$

where T^{-1} is the inverse matrix of T, which can be directly measured for pure chemical species with our system to serve as the calibration data. From Equations (1)–(3), it is clear that, with N-color SRS imaging, M chemical species can be retrieved quantitatively when $N = M$. Note that, with $N > M$, an overdetermined system will improve the detection sensitivity.

We use a linear combination of signals at different vibrational frequencies for quantitative multicolor tissue imaging. Figures 3(a) and (b) show the simultaneous SRS images of mouse ear skin at 2940 cm^{-1} and 2845 cm^{-1}, corresponding to the CH_3 stretching vibration for protein-rich mapping and the CH_2 stretching vibration for lipid-rich mapping, respectively [20]. However, as shown in Figure 3(c), lipid and protein have severe Raman band overlapping, indicating that the chemical specificity in Figures 3(a) and (b) is poor. Based on Equations (1)–(3), with two-color SRS images and the pure protein and lipid calibration data, protein ($[c]_{protein} \propto 5.2S_1 - 4.16S_2$) and lipid ($[c]_{lipid} \propto 1.2S_2 - 0.3S_1$) in the tissue can be quantitatively retrieved with high chemical selectivity, as shown in Figures 3(d) and (e), respectively. In the protein channel (Figure 3(d)), the hair, which is protein-rich, generates stronger signals, while in the lipid channel (Figure 3(e)), the signal from the aggregated lipids surrounding the hair, secreted by the sebaceous gland, is much stronger than from the hair itself. Figure 3(f) is a composite image of the skin protein (red) and lipids (green), which clearly reveals their relative spatial distributions. From the intensity profile across the line indicated in Figure 3(f) as shown in Figure 3(g), protein and lipid are clearly distinguished with the linear combination calculation. Figure 3(h) shows the reconstructed three-color image of the skin sample at a deeper depth (~50 μm). Condensed fat cells are visualized, between which there are protein-rich network structures. Note that the third-color image at 2780 cm^{-1}, corresponding to the non-Raman background (magenta bar in Figure 3(c)), is applied to detect the two-color TPA signals from blood (magenta). These TPA signals will appear in all three channels, making it very convenient for removal through digital background subtraction. Simultaneous three-color SRS imaging of skin

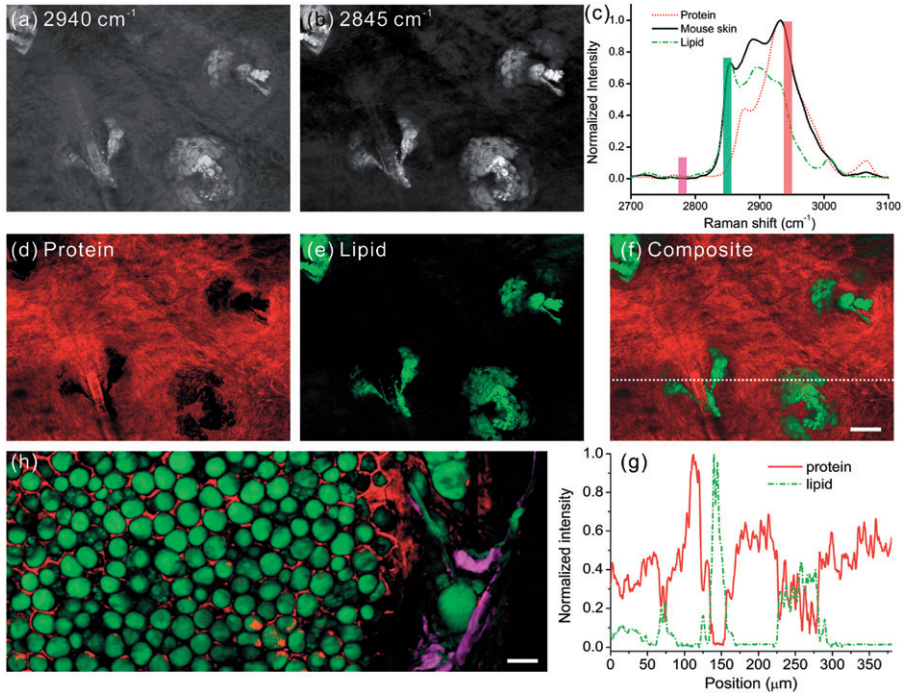

Figure 3. Simultaneous two-color SRS images of fresh mouse ear skin at (a) 2940 cm^{-1} and (b) 2845 cm^{-1} at a depth of ~15 μm. (c) Raman spectra of lipid, protein and the mouse skin. By calculation using Equations (1)–(3), the pure protein and lipid distributions could be quantitatively retrieved from the two-color images ((a) and (b)), as shown in (d) and (e), respectively. (f) Overlay of (d) and (e). (g) The intensity profile across the line indicated in (f) for both protein and lipid. (h) Overlapped distribution of lipid (green), protein (red) and blood (magenta) retrieved from the simultaneous three-color images (SRS or TPA) from the same sample at a depth of ~50 μm with 2940 cm^{-1}, 2845 cm^{-1} and 2780 cm^{-1}. The average power of each peak in the comb-shape spectrum of the sample is ~15 mW. The scale bar is 20 μm.

provides the co-distribution of different chemical species, and may become a valuable tool for the quantitative study of dermatologic diseases, or for real-time monitoring of drug delivery efficiency to the skin [21,22].

4. Discussion and conclusion

In this paper we present a multicolor SRS microscopic imaging technique. Multicolor imaging at a few particular Raman vibrational resonances of interest is acquired simultaneously, and pure chemical species are quantitatively retrieved using a linear combination calculation. This method possesses several advantages. First, the simultaneous acquisition of multicolor images ensures the exact co-localization or relative spatial distribution of different Raman oscillators across the sample. Secondly, since different channels are working in parallel independently, there is no additional limit on the scanning speed for label-free SRS imaging, which allows rapid imaging. Third, in our experiment, the strip scanning method is used. For 2D mosaic imaging, this method is superior because of the absence of intensity heterogeneity in the stage moving direction compared with the traditional square tiling method [19]. As another advantage, along the stage scanning direction, strip scanning, up to one centimetre, can be readily realized with a much fast acquisition speed (data not shown).

Note that the number of multicolor channels is extendable, but is limited by two factors: one is the restricted spectral bandwidth of the fs laser source, and the other is the limited channels in the lock-in amplifier due to its current high cost. More channels provide more chemical contrasts from the same specimen, and, in the extreme case, realized with a high-density photodiode and lock-in amplifier array, the full SRS spectra with high sensitivity can also be acquired in parallel, which may play a more important role in biological and biomedical applications compared with narrowband imaging. Alternatively, with several synchronized picosecond optical parametric oscillators (OPOs) or optical parametric amplifiers (OPAs), instead of the spectrally tailored fs laser source, the spectral resolution of each peak could be dramatically

improved to 3–5 cm^{-1}. We applied our system to image freshly excised mouse ear skin, but for too thick tissue samples with high heterogeneity, multi-scattering may cause crosstalk between adjacent detectors, which remains one limitation of the technique at the current stage. Although the power on the sample in our method is relatively higher than for single-color imaging, we did not observe clear photobleaching or photodamage with the power we used in our experiment.

In conclusion, we demonstrate a simultaneous multicolor SRS microscopic technique with a grating-based pulse shaper for excitation and a grating-based spectrograph for detection for tissue imaging and the quantitative retrieval of different chemical species with multiple chemical-selective contrasts. In particular, this technique can be used for multi-parametric SRS flow cytometry, in which simultaneous detection is mandatory. It is expected that, with increased channels and improved spectral resolution, this technique could find more applications in complex and important biological and biomedical systems.

Acknowledgements

We thank Zhibo Wang and Xu Zhang for their help with the mouse tissue sample preparation, and Terumasa Ito and Wenlong Yang for technical discussions. This work was supported by the U.S. Department of Energy's Basic Energy Sciences Program (DE-SC001548) and the National Institute of Health's T-R01 (1R01EB010244-01) awarded to X.S.X.

References

[1] C.W. Freudiger, W. Min, B.G. Saar, S. Lu, G.R. Holtom, C. He, J.C. Tsai, J.X. Kang and X.S. Xie, Science **322**, 1857 (2008).
[2] B.G. Saar, C.W. Freudiger, J. Reichman, C.M. Stanley, G.R. Holtom and X.S. Xie, Science **330**, 1368 (2010).
[3] E.R. Andresen, P. Berto and H. Rigneault, Opt. Lett. **36**, 2387 (2011).
[4] H.T. Beier, G.D. Noojin and B.A. Rockwell, Opt. Express **19**, 18885 (2011).
[5] A. Folick, W. Min and M.C. Wang, Curr. Opin. Genet. Dev. **21**, 585 (2011).
[6] H. Frostig, O. Katz, A. Natan and Y. Silberberg, Opt. Lett. **36**, 1248 (2011).
[7] A. Gambetta, V. Kumar, G. Grancini, D. Polli, R. Ramponi, G. Cerullo and M. Marangoni, Opt. Lett. **35**, 226 (2010).
[8] Q. Liu, Z. Ouyang and S. Albin, Opt. Express **19**, 4795 (2011).
[9] Y. Ozeki, Y. Kitagawa, K. Sumimura, N. Nishizawa, W. Umemura, S. Kajiyama, K. Fukui and K. Itoh, Opt. Express **18**, 13708 (2010).
[10] V.V. Yakovlev, G.D. Noojin, M.L. Denton, B.A. Rockwell and R.J. Thomas, Opt. Lett. **36**, 1233 (2011).
[11] Y.R. Shen, *The Principles of Nonlinear Optics* (Wiley, New York, 1984).
[12] W. Min, C.W. Freudiger, S. Lu and X.S. Xie, Annu. Rev. Phys. Chem. **62**, 507 (2011).
[13] B.G. Saar, Y. Zeng, C.W. Freudiger, Y.S. Liu, M.E. Himmel, X.S. Xie and S.Y. Ding, Angew. Chem. **49**, 5476 (2010).
[14] P. Tian and W.S. Warren, Opt. Lett. **27**, 1634 (2002).
[15] M.N. Slipchenko, H. Chen, D.R. Ely, Y. Jung, M.T. Carvajal and J.X. Cheng, Analyst **135**, 2613 (2010).
[16] C.W. Freudiger, W. Min, G.R. Holtom, B.W. Xu, M. Dantus and X.S. Xie, Nature Photon. **5**, 103 (2011).
[17] D. Fu, F. Lu, X. Zhang, C.W. Freudiger, D.R. Pernik, G.R. Holtom and X.S. Xie, J. Am. Chem. Soc. **134**, 3623 (2012).
[18] F. Lu, W. Zheng, J. Lin and Z.W. Huang, Appl. Phys. Lett. **96**, 133701 (2010).
[19] S. Abeytunge, Y.B. Li, B. Larson, R. Toledo-Crow and M. Rajadhyaksha, J. Biomed. Opt. **16**, 050504 (2011).
[20] B.G. Saar, R.S. Johnston, C.W. Freudiger, X.S. Xie and E.J. Seibel, Opt. Lett. **36**, 2396 (2011).
[21] B.G. Saar, L.R. Contreras-Rojas, X.S. Xie and R.H. Guy, Mol. Pharm. **8**, 969 (2011).
[22] D. Zhang, M.N. Slipchenko and J.X. Cheng, J. Phys. Chem. Lett. **2**, 1248 (2011).